Exact Spiral Scan Region-of-Interest Cone Beam CT Via Backprojection

K.C. Tam[a], G. Lauritsch[b], and K. Sourbelle[c]
[a]Siemens Corporate Research, Inc. Princeton, NJ 08540
[b]Siemens AG, Medical Engineering Group, Erlangen, Germany
[c]Institute of Medical Physics, University of Erlangen, Erlangen, Germany

Abstract

We present a spiral scan cone beam reconstruction algorithm in which image reconstruction proceeds via backprojection in the object space. In principle the algorithm can reconstruct sectional ROI in a long object. The approach is a generalization of the cone beam backprojection technique developed by Kudo and Saito in two aspects: the resource-demanding normalization step in the Kudo and Saito's algorithm is eliminated through the technique of data combination which we published earlier, and the elimination of the restriction that the detector be big enough to capture the entire image of the ROI. Restricting the projection data to the appropriate angular range required by data combination can be accomplished by a masking process. Because of the simplification resulting from the elimination of the normalization step, the most time-consuming operations of the algorithm can be approximated by the efficient step of line-by-line ramp filtering the cone beam image in the direction of the scan path, plus a correction image. The correction image, which can be computed exactly, is needed because data combination is not properly matched at the mask boundary when ramp filtering is involved. Empirical 2D PSF, the Shepp-Logan filter, and a modified ramp filter are developed to improve matching with the correction image which is computed with finite samplings. The use of transition region to further improve matching is introduced. The results of testing the algorithm on simulated phantoms are presented.

I. INTRODUCTION

In [1, 2] we presented a backprojection algorithm for spiral scan cone beam CT to reconstruct a sectional region-of-interest (ROI) in a long object from cone beam (CB) data acquired on a detector shorter than the ROI without contamination by the overlaying materials. The x-ray source scans the ROI along a spiral scan path, with a top circle scan at the top level of the ROI and a bottom circle scan at the bottom level of the ROI. The only height requirement on the detector is that it should be longer than the distance between adjacent turns in the spiral. The algorithm is a modofication of the Radon-space driven data-combination technique for ROI cone beam image reconstruction developed in our prior works [3 ,4]. In the Radon-space technique the radial Radon derivative for each plane intersecting the ROI is obtained by combining the partial results computed from the cone beam data at the various source positions that the plane intersects. This data-combination technique is illustrated in Figure 1 which represents a plane Q intersecting the ROI and the scan path. Since the partial planes do not overlap and together they completely cover the portion of plane Q that lies within the ROI, the Radon derivative for plane Q can be obtained exactly by summing the Radon derivatives for the partial planes. After all the Radon derivatives are computed in this way, the image is obtained by inverse Radon transformation.

In [1, 2] this Radon-space driven data-combination algorithm was modified so that image reconstruction proceeds via backprojection in the object space. This is achieved by generalizing the cone beam backprojection technique developed by Kudo and Saito [5]. The Kudo and Saito algorithm essentially consists of the following 6 steps: (1) 2D projection of the cone beam image at all angles; (2) spatial derivative of the projections; (3) normalization of the projection derivatives; (4) 2D backprojection of the normalized projection derivative from all angles; (5) derivative of the resulting backprojection image in the scan path direction. The result of steps (1) through (5) is a filtered cone beam image. Finally in step (6) the filtered cone beam image is 3D backprojected into the object space. This 6-step algorithm suffers from two limitations: it requires the use of a normalization function $M(r,\theta)$ which depends on the source position as well as the 2D projection coordinates (r,θ); and it requires that the detector to be big enough to capture the entire image of the ROI.

II. NORMALIZATION VIA DATA COMBINATION

In our previous works we have developed an approach [6,7] which eliminates both of these two limitations. Instead of division by the function $M(r,\theta)$, normalization of the reconstructed object densities is achieved through the data-combination method developed in [3 ,4]. At each cone beam view the projection operations (i.e. line integrations) in step (1) are restricted to only the cone beam data bound by the angular ranges as indicated in Figure 1. In this way the totality of the cone beam data from all the contributing source positions covers any plane of integration in its entirety without any overlap. Therefore with this arrangement the normalization function $M(r,\theta)$ can be set to unity for all cone beam views.

Restricting the projection data to the appropriate angular range can be accomplished by a masking process. The mask consists of a top curve and a bottom curve formed by projecting the spiral turn above and the turn below from the

0-7803-5696-9/00/$10.00 (c) 2000 IEEE

current source position. It can be easily seen that such masking procedure corresponds exactly to the angular range bound by the prior and the subsequent source positions as indicated in Figure 1. We shall refer to this mask as the data-combination mask. For the reconstruction of a sectional ROI in a long object, circular arc scans are needed at the top and bottom levels. The addition of the 2 circle scans to the spiral scan enables the sectional ROI to be reconstructed without contamination by the overlaying materials. These masks have been detailed in [3,4].

With $M(r,\theta) = 1$ due to data combination via masking, it becomes practical to implement the Kudo and Saito's 6-step algorithm to reconstruct images from spiral scan data. Care should be exercised in carrying step (2). Each integration line L intersecting the masked cone beam image corresponds to a partial plane as depicted in Figure 1. The computation of the Radon derivative of the partial plane is achieved by computing the integrals on 2 adjacent line segments L_1 and L_2 closely spaced from L; the difference between the integrals computed on L_1 and L_2 yields the correct Radon derivative, up to a multiplicative constant. For the result to be valid, the angle subtended by the partial plane at the source position should remain unchanged at L_1 and L_2. By taking partial derivative of the line segment length w.r.t. the translation spacing between L_1 and L_2, it can be shown that the change Δt in the integration line segment t is given by the expression:

$$\Delta t = \frac{\sin\alpha_0 \cos\alpha_0}{a} t \Delta s \qquad (1)$$

where α_0 is the angle the partial plane makes with the normal from the source to the detector, a is the distance of the source from the detector, and Δs is the spacing between the 2 lines on the detector where the partial plane intersects before and after rotation. Equation (1) was first derived by Kudo et al [8] using a different approach.

Equation (1) can be approximately satisfied with L_1 and L_2 generated by translating L sideway orthogonally. We shall refer to this way of masking as soft masking. The degree to which soft masking approximates Equation (1) is a function of cone angle; in our experience it works very well up to a few degree. Soft masking is the procedure used in the reconstructions in the Radon-space driven approach we previously presented in [3,4]. Soft masking is also implied when line integral derivative is computed by performing line integration on the derivatives of the cone beam image [8] instead of on the cone beam image itself. It is understood here that for a cone beam view on a circle scan imaging a sectional ROI of a long object, the portion of L_1 and L_2 outside the portion of the mask boundary defined by the respective circle scan would make no contribution to the line integrals because the sectional ROI has zero densities beyond the circle scan.

With steps (1) and (2) in the Kudo and Saito's 6-step algorithm replaced by soft masking and the normalization step (i.e. step (3)) eliminated because $M(r,\theta) = 1$ from data combination, the reconstruction algorithm now consists of four steps: (1) soft masking at all angles; (2) backprojection of the projection derivative from all angles; (3) derivative of the resulting backprojection image in the scan path direction; and (4) 3D backprojection into the object space. This algorithm was referred to as the four-step algorithm [1,2,7].

III. Line Integration Limits

If integration is performed on line segments intersecting the masked cone beam image, the line segments are truncated by the mask. The integration line limits set in this way obviously violates Equation (1) in computing the Radon derivative of a partial plane. We shall refer to this way of setting the line integral limits as hard masking. Consider the line integral limit decomposition:

$$\begin{aligned}\text{Exact line integral limit} &= \text{Hard masking} + (\text{Exact line integral limit} - \text{Hard masking}) \\ &= \text{Hard masking} + \text{Correction line integral limit}\end{aligned} \qquad (2)$$

where correction line integral limit is defined as the difference between exact line integral limit (according to Equation (1)) and hard masking. When the four-step algorithm is applied to the cone beam image together with the decomposition in Equation (2) two images are generated, which we shall refer to as the hard masking image and the correction image. The advantage of incorporating the line integral limit decomposition is that it can be shown [1,6] that in the case of the hard masking term in Equation (2) the first three steps in the four-step algorithm is equivalent to the efficient space invariant line-by-line ramp filter in the direction of the scan path. A similar approach was presented in Kudo et al [8] to reconstruct from truncated spiral scan data.

The correction image is computed by applying the four-step algorithm to the difference between exact line integral limit and hard masking. Note that the 2D projection operation for the correction image can be carried out much faster than for the entire cone beam image, since it involves only a small portion of the cone beam image bordering the mask boundary. Note also that backprojection from each line segment should be extended to the virtual detector which is high enough to cover the entire ROI, rather than the actual short detector, as already pointed out before [1,2,6,8].

IV. Convolution Filtering

In our implemention of the line integral limit decomposition, the cone beam image is partitioned into an interior region not intersecting the mask boundary and a region bordering the mask boundary. The two regions are

partitioned along pixel edges to facilitate computation. Let $M_{int}(x,y)$ be the support function of the interior region. The interior image, which is the product of the cone beam image with the support $M_{int}(x,y)$, is filtered with a space invariant filter, and the small portion of the cone beam image bordering the mask boundary, which is the product of the cone beam image with the support $(1-M_{int}(x,y))$, is filtered with the 4-step algorithm, and finally the two filtered images are combined. We shall refer to this approach as the combination method. The combination method was first disclosed in [9]. In practice the different behavior of the two filtering operations with respect to numerical implementation causes mismatch and instability when the two filtered images are combined.

To reduce mismatch between the convolution filtered result of the interior image and the 4-step algorithm filtered result of the image bordering the mask boundary, a "transition region" was inserted between the two regions. A weighting map $M_c(x,y)$ is generated by convolving the support $M_{int}(x,y)$ of the interior region with a m x m smoothing window, where m is a small integer. The values of $M_c(x,y)$ then lies between 0 and 1. Whereas the transition from a value of 1 to 0 at the edge is abrupt for $M_{int}(x,y)$, the transition for $M_c(x,y)$ is more gradual. A transition region is thus inserted between the two regions undergoing different filtering operations, as illustrated in Figure 2. The combination method including transition region now works as follows. The product of the cone beam image with $M_c(x,y)$ is filtered with the convolution technique, and the product of the cone beam image with $(1-M_c(x,y))$ is filtered with the 4-step algorithm. Then the two results are combined. In this way the 4-step algorithm filtered result and the convolution filtered result are merged less abruptly by including the contributions from both filterings in the transition region between the two regions. If the "half width" of the m x m smoothing window is smaller than the width between the mask boundary and the edge of the interior region, the support of $M_c(x,y)$ will be smaller than the data-combination mask. Consequently unlike the technique employed by Kudo et al [8], the method does not require a detector larger than that implied by data combination, and therefore no x-ray data beyond the mask boundary are needed.

In principle the PSF of the 4-step filtering algorithm is a 1D ramp filter when applied with infinite samplings. However finite samplings result in a low-pass filtered modification of the ramp filter as can be seen in the Fourier transform of the empirical PSF in Figure 3, which degrades the spatial resolution in the reconstruction images. In addition, in spatial domain the filter kernel suffers a small spread of about 3 lines in the vertical dimension. We investigated the Shepp-Logan kernel as well as the ramp filter convolved by a Hamming window for use as filter kernel in place of the empirical PSF. In Figure 3 is shown the spectral behavior of these kernels. The Shepp-Logan kernel yields the highest spatial resolution, but requires the widest transition region of width=11 compared to width=3 when using the empirical PSF. Both 1D and 2D filter kernels were included in our study, the latter are generated by spreading the corresponding 1D filter kernels in the manner in the empirical 2D PSF.

To some degree the spatial resolution degradation in the horizontal dimension (parallel to spiral tangent) caused by finite samplings can be reduced by high-pass filtering the filtered cone beam image. The high-pass filter function $F_{highpass}(\omega)$ is obtained from:

$$F_{\text{highpass}}(\omega) = \frac{F_{\text{total filter}}(\omega)}{F_{PSF}(\omega) + \varepsilon}$$

where $F_{total\ filter}(\omega)$ is the desired total filter function, $F_{PSF}(\omega)$ the empirical PSF and ε a regularization constant. As an example Figure 4 shows a 1D high-pass kernel which leads to a modified 2D Shepp-Logan filter (see Figure 3) as the total filter function. The computational expense of high-pass filtering is negligible compared to that of other steps in the combination method.

V. VALIDATION

The reconstruction algorithms were validated on the 3D Shepp-Logan Phantom. The spiral scan radius is 30 cm, and the spiral pitch is 10 cm. There are 300 views per rotation. The detector has 256 x 128 elements each of dimensions $(0.09\ cm)^2$. The effective cone (half) angle is 4.8^0. The output region contains 256 x 256 x 256 voxels each of $(0.078\ cm)^3$.

A longitudinal cross-section of the image reconstructed using the 4-step algorithm is shown in Figure 5A. For the combination method combining 1D or 2D convolution filtering and 4-step algorithm filtering reconstructed images are shown in Figure 5B-5E for various filter kernels. The width of the transition region was width=11 for all filter kernels. Using the empirical 2D PSF as a filter kernel the reconstruction shown in Figure 5B is essentially identical to the one reconstructed entirely with the 4-step algorithm as shown in Figure 5A. When using a ramp filter convolved by a Hamming window the spatial resolution of the reconstruction shown in Figure 5C is increased significantly, as is reflected in the spectral behavior of the filter function in Figure 3. The Shepp-Logan kernel yields an additional improvement in spatial resolution, see Figure 5D. Eliminating the vertical spread of the kernel and strictly using a 1D Shepp-Logan kernel has an impact on spatial resolution in the vertical direction (Figure 5E). Application of the high-pass kernel of Figure 4 (which leads to a modified 2D Shepp-Logan filter, see Figure 3) yielded image quality which is comparable to that of the combination method with the 2D Shepp-Logan filter as filter function, see Figure 5F and 5D, respectively. In our yet-to-be optimized implementation the use of convolution filtering speeded up the reconstruction process by an order of magnitude.

VI. DISCUSSION

We have presented a spiral scan cone beam reconstruction algorithm in which image reconstruction proceeds via backprojection in the object space. In principle the algorithm can reconstruct sectional ROI in a long object. A convolution method was developed to speed up the reconstruction process. Matching of the convolved cone beam data with the correction image was achieved by the use of a transition region. We showed that a variety of filter kernels can be used to meet the tradeoff between spatial and contrast resolution requirements of any particular application. In addition we presented an alternative high-pass filtering approach on the filtered cone beam image to increase spatial resolution. Both approaches achieved comparable image results on simulated phantom reconstructions.

Further improvement in image quality and reduction in reconstruction time could come as a result of improvement in modelling the transition region, the filter kernels and more optimized numerical operations. They are the subjects of further investigations.

VII. ACKNOWLEDGMENTS

This work was supported in part by Bavarian Research Consortium of Medical Imaging (FORMED).

VIII. REFERENCES

[1] K.C. Tam, B. Ladendorf, F. Sauer, G. Lauritsch, and A. Steinmetz, "Backprojection spiral scan region-of-interest cone beam CT", *Proc. SPIE Medical Imaging 1999: Physics of Medical Imaging*, pp. 433-441, 1999.

[2] K.C. Tam, G. Lauritsch, K. Sourbelle, F. Sauer, and B. Ladendorf, "Exact Spiral Scan Region-of-Interest Cone Beam Reconstruction via Backprojection", *Proc. 1999 International Meeting on Fully Three-Dimensional Image Reconstruction in Radiology and Nuclear Medicine*, The Netherlands, June 23-26, pp.15-18, 1999.

[3] K.C. Tam, "Helical and circle scan region of interest computerized tomography", *US. Patent* 5,463,666, Oct 31, 1995.

[4] K.C. Tam, S. Samasekera, and F. Sauer, "Exact Cone Beam CT with A Spiral Scan", *Phys. Med. Biol.*, 43, pp. 1015-1024, 1998.

[5] H. Kudo and T. Saito, "Derivation and Implementation of a Cone-Beam Reconstruction Algorithm for Nonplanar Orbits", *IEEE Trans.Med. Imag.*, MI-13, pp. 196-211, 1994.

[6] K.C. Tam, "Mask Boundary Correction in FBP Spiral Scan Cone Beam Imaging System". Siemens Corporate Research Invention Disclosure IPD 97E9203 US; Nov 6, 1997.

[7] K.C. Tam, "Exact region of interest cone beam imaging using 3D backprojection", *US. Patent* 5,926,521, July 20, 1999.

[8] H. Kudo, F. Noo, and M. Defrise, "Cone-beam filtered-backprojection algorithm for truncated helical data", *Phys. Med. Biol.*, 43, pp. 2885-2909, 1998.

[9] F. Sauer, K.C. Tam, and B. Ladendorf, "Pixel Grouping For Filtering Cone Beam Detector Data During 3D Image Reconstruction", US Patent Application serial number 09/163,494, filed on September 30, 1998.

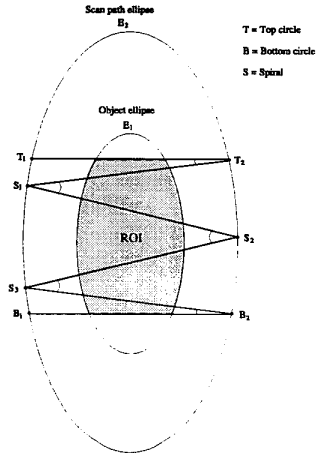

Figure 1. A typical integration plane covering the ROI defined by the source positions.

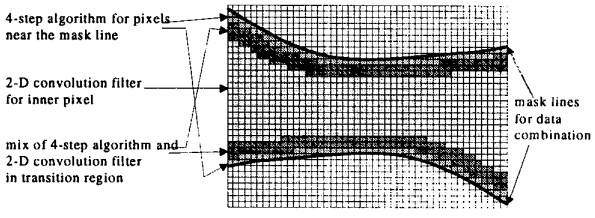

Figure 2. Dividing the cone beam image into regions for different methods of filtering.

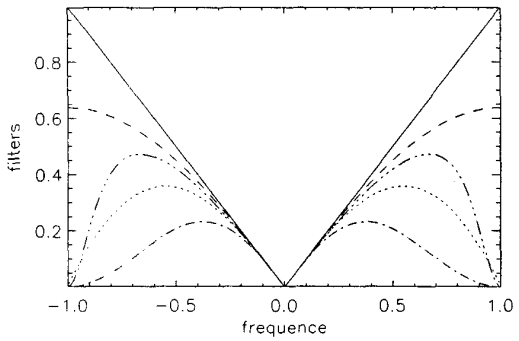

Figure 3. Spectral plots of various filter kernels in the horizontal direction (parallel to spiral tangent): empirical PSF (dashed dotted line), ramp filter convolved with a Hamming window (dotted line), Shepp-Logan filter (dashed line), modified Shepp-Logan filter (dashed double dotted line), ramp filter (solid line).

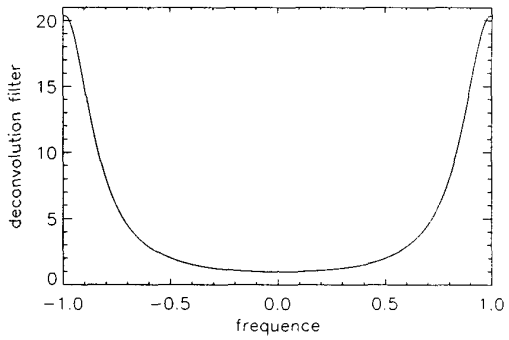

Figure 4. Spectral plot of a high-pass kernel to obtain a modified Shepp-Logan filter as total filter function.

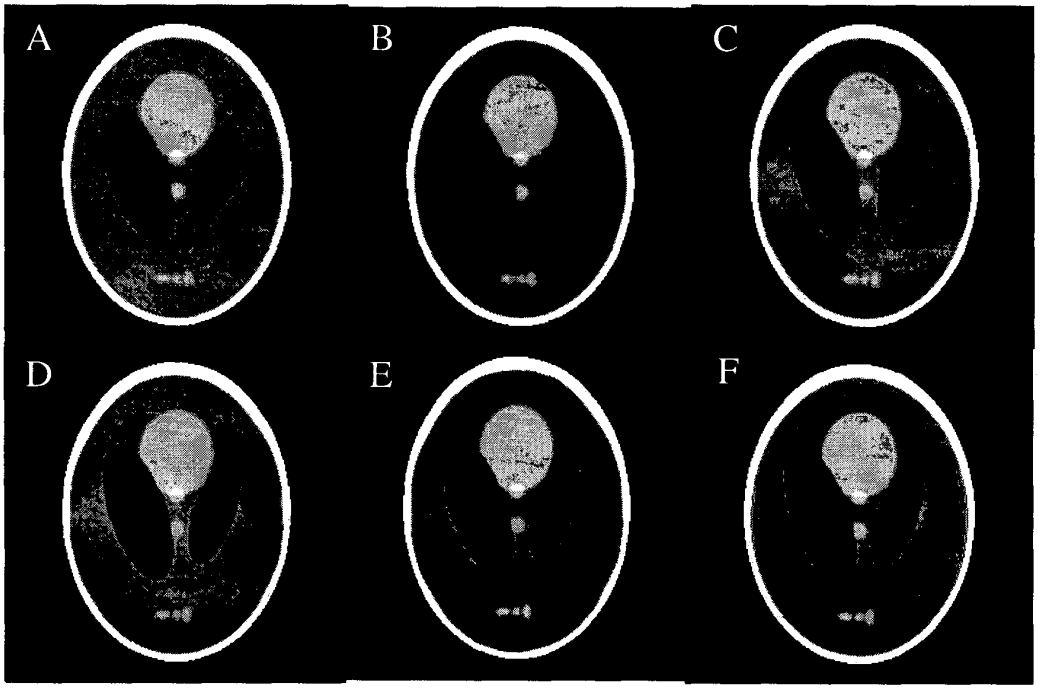

Figure 5. A longitudinal cross-section of the image of the simulated Shepp-Logan phantom reconstructed: A. using the four-step algorithm; B through E: using the combination method with as the filter kernel: B. the empirical 2D PSF of the 4-step algorithm; C. a 2D ramp filter convolved by a Hamming window; D. a 2D Shepp-Logan filter; E. a 1D Shepp-Logan filter; F. using the four-step algorithm followed by high-pass filtering so as to yield a modified 2D Shepp-Logan filter as total filter function.